Formation of the compact jets in the black hole GX 339−4.

S. Corbel[1]⋆, H. Aussel[1], J. W. Broderick[2], P. Chanial[1], M. Coriat[2], A. J. Maury[3],
M. Buxton[4], J. A. Tomsick[5], A. Tzioumis[6], S. Markoff[7], J. Rodriguez,[1] C. Bailyn[4],
C. Brocksopp[8], R. Fender[2], P.O. Petrucci[9], M. Cadolle-Bel[10], D. Calvelo[2], L. Harvey-Smith[6]

[1] *Laboratoire AIM (CEA/IRFU - CNRS/INSU - Université Paris Diderot), CEA DSM/IRFU/SAp, F-91191 Gif-sur-Yvette, France*
[2] *School of Physics and Astronomy, University of Southampton, Highfield, Southampton, SO17 1BJ, UK*
[3] *ESO, Karl Schwarzschild Strasse 2, 85748, Garching bei Munchen, Germany*
[4] *Astronomy Department, Yale University, P.O. Box 208101, New Haven, CT 06520-8101, USA*
[5] *Space Sciences Laboratory, 7 Gauss Way, University of California, Berkeley, CA 94720-7450, USA*
[6] *CSIRO Astronomy & Space Science, Australia Telescope National Facility, PO Box 76, Epping NSW 1710, Australia*
[7] *Astronomical Institute 'Anton Pannekoek', University of Amsterdam, PO Box 94249, 1090 GE Amsterdam, the Netherlands*
[8] *Mullard Space Science Laboratory, University College London, Holmbury St Mary, Dorking, Surrey RH5 6NT, UK*
[9] *UJF-Grenoble 1/CNRS-INSU, Institut de Planétologie et d'Astrophysique de Grenoble (IPAG) UMR 5274, Grenoble F-38041, France*
[10] *ESAC/ISOC, P.O. Box 78, 28691 Villanueva de la Cañada, Spain.*

ABSTRACT
Galactic black hole binaries produce powerful outflows with emit over almost the entire electromagnetic spectrum. Here, we report the first detection with the *Herschel* observatory of a variable far-infrared source associated with the compact jets of the black hole transient GX 339−4 during the decay of its recent 2010-2011 outburst, after the transition to the hard state. We also outline the results of very sensitive radio observations conducted with the Australia Telescope Compact Array, along with a series of near-infrared, optical (OIR) and X-ray observations, allowing for the first time the re-ignition of the compact jets to be observed over a wide range of wavelengths. The compact jets first turn on at radio frequencies with an optically thin spectrum that later evolves to optically thick synchrotron emission. An OIR reflare is observed about ten days after the onset of radio and hard X-ray emission, likely reflecting the necessary time to build up enough density, as well as to have acceleration (e.g. through shocks) along an extended region in the jets. The *Herschel* measurements are consistent with an extrapolation of the radio inverted power-law spectrum, but they highlight a more complex radio to OIR spectral energy distribution for the jets.

Key words: accretion, accretion disks – black holes physics – X-rays: binaries – ISM: jets and outflows – stars: individual (GX 339-4).

1 INTRODUCTION

During outbursts of X-ray binaries, an enormous amount of accretion energy is harnessed to produce powerful jets (e.g. Fender 2006). For a very long time, those jets were only detected in radio (e.g. Hjellming, Gibson & Owen 1975; Mirabel et al. 1992). However, the recent decade demonstrated that relativistic jets from black holes (hereafter BH) and neutron stars are multi-wavelength emitters with emission even up to γ rays (Laurent et al. 2011; Corbel et al. 2012b). Powerful self-absorbed compact jets (Fender 2001) are observed in the hard state of BH binaries, and are reminiscent of those found in active galatic nuclei. Models of

compact jets (Blandford & König1 1979; Falcke & Biermann 1995) predict that their spectral energy distributions (SED) should be a flat or slightly inverted power-law between the radio and a turnover frequency estimated in the mid to near-infrared (NIR) for Galactic BHs (Corbel & Fender 2002; Gandhi et al. 2011; Russell et al. 2012b). Such NIR synchrotron excess emission from the jets has now been detected in a growing number of BH transients (e.g. Jain et al. 2001; Buxton & Bailyn 2004; Buxton et al. 2012; Dinçer et al. 2012; Russell et al. 2012a). However, there is almost an unexplored four decades frequency gap between the radio and the NIR domains. Only very few millimeter and mid-infrared (IR) observations (e.g. Fender et al. 2001; Migliari et al. 2007; Gallo et al. 2007; Rahoui et al. 2011; Gandhi et al. 2011) have been conducted in this range and
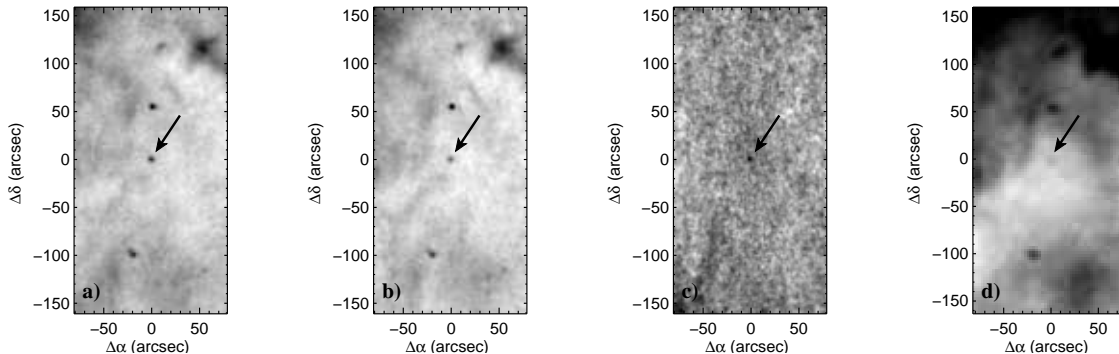
⋆ E-mail:stephane.corbel@cea.fr

Figure 1. *Herschel* maps of GX 339−4: at 70 μm on Feb. 25 (a) and Mar. 6 (b), their difference in (c), and at 160 μm (2 epochs) in (d).

usually with very limited sensitivity. New theoretical calculations highlight the possibility of a more complicated spectral shape (Pe'er & Casella 2009), especially in the far to NIR range. Strong variability can be observed in the NIR on short timescale ($\sim$ seconds) allowing one to probe physical changes at the base of the jet. These variations seem to vanish on longer timescales (above a few hundreds seconds, Casella et al. 2010; Gandhi et al. 2011; Rahoui et al. 2012).

This points to the importance of sensitive submillimeter to far-IR observations that can only bridge the gap between the radio and the NIR ranges. In this Letter, we report the first far-IR observations with the ESA *Herschel* satellite of the recurrent binary GX 339−4 during the decay of its recent outburst in 2011. GX 339−4 is believed to harbour a BH with a mass > 7 $M_\odot$ (Hynes et al. 2003; Muñoz-Darias, Casares & Martínez-Pais 2008) in a system with a low mass star companion, and located at a likely distance of 8 kpc (Zdziarski et al. 2004). In Section 2, we describe the *Herschel* observations along with complementary radio, NIR, optical and X-ray observations. The detailed multi-wavelength lightcurves, as well as the far-IR detections, are also presented and these results are discussed in Section 3.

2 OBSERVATIONS AND RESULTS

2.1 Herschel far-infrared Observations

Following the transition of GX 339−4 back to the hard state during the decay of its 2010-11 outburst, we triggered two DDT (Director Discretionary Time) observations with the *Herschel* satellite[1] (Pilbratt et al. 2010). GX 339−4 was observed with the PACS instrument (Poglitsch et al. 2010) at 70 μm and 160 μm on 2011, February 25 and March 6 (Table 1). We used a sequence of two so-called "mini-scan map" mode, providing an area of 50" in diameter with homogenous coverage for a total on-source time of 1152 s. The data were processed with `HCSS` version 6.0.1106 and we reconstructed the maps with the `Tamasis` software (Chanial et al. in prep)[2]. As GX 339−4 sits in the Galactic plane in the

Obs. ID	Date	f_ν (70 μm) (mJy)	f_ν (160 μm) (mJy)
1342215720	2011-02-25	21.0 ± 1.0	13.2 ± 4.6
1342215721	2011-02-25		
1342216156	2011-03-06	13.9 ± 1.0	
1342216157	2011-03-06		

Table 1. *Herschel* observations log of GX 339−4

midst of a strong cirrus background, we paid a special attention in the map reconstruction to preserve the structure of the background. The resulting flux density maps at 70 μm are shown in Fig. 1 (a, b). A point source is clearly detected at the center of each map, as well as some extended emission across the field. A single point source is visible in the difference image (Fig. 1c) at the center, clearly indicating the detection at 70 μm of a variable source at the location of GX 339−4. All the other sources and structure have been subtracted out. In order to choose the optimum apertures for source and sky extraction, calibrate our photometry and check the impact of the varying cirrus background, we have run a set of simulations, where point sources were added to the bolometer timelines by applying our observation model to the observed PACS point spread function of Lutz (2012). We reconstructed the maps and performed aperture photometry on the simulated sources and GX 339−4, with various aperture size and sky annuli. We selected the combination giving the highest signal to noise for point sources (Table 1). The cirrus confusion noise adds 0.77 mJy at 70 μm and 4.5 mJy at 160 μm in quadrature to the point source sensitivity. As a result, we only obtain a 2.9 σ detection at 160 μm by combining the two observations, while GX 339−4 is detected at high significance at 70 μm in each epoch.

2.2 Radio, OIR and X-ray observations

In order to probe the evolution of the SED from the compact jets, the *Herschel* observations were included in a large campaign of multi-wavelength observations. All radio observations were performed with the Australia Telescope Compact Array (ATCA) located in Australia. The ATCA observations were conducted at 5.5 and 9 GHz (also at 2.2 GHz during the first *Herschel* run) with the upgraded and sensitive CABB back-end (see Table 2 available as online support-
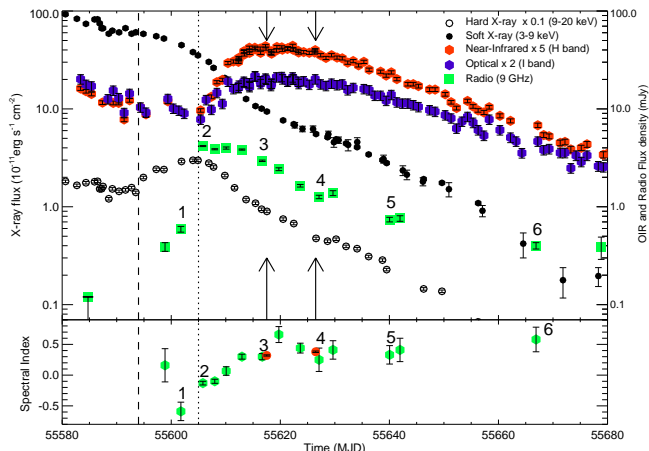
Figure 2. (Top): The lightcurves (with multiplicative factors as indicated in the legend) of GX 339−4 during the decay of the 2010-11 outburst in radio (green), NIR (red), optical (purple), soft X-ray (filled black circle) and hard X-ray (open black circle). The arrows highlight the *Herschel* observations (observations # 3 and 4). (Bottom): Evolution of the radio (green hexagon) 5.5 to 9 GHz spectral index (see text) once GX 339−4 initiated its transition back to the hard state. The radio to far-IR spectral indices using the *Herschel* data) are represented by the red circle. The dashed line indicates the transition back to the hard state according to Dinçer et al. (2012). The vertical dotted line highlights the onset of OIR emission close to the peak of hard X-ray and radio emission. The numbers refer to the individual observations displayed in Fig. 3.

ing information). The PCA and XRT detectors onboard the *RXTE* and *Swift* satellites provide the X-ray coverage during the soft to hard state transition. Further details on the radio and X-ray data analysis can be found in Corbel et al. (2012a). The optical and near-infrared (herafter OIR) observations were taken with the ANDICAM camera on the SMARTS 1.3 m telescope located at Cerro Tololo in Chile (see Buxton et al. 2012). Images in H, J, I and V filters are obtained on a near-daily basis when GX 339−4 is visible in the night sky. The magnitudes have been converted to flux units using a total extinction of $A_V = 3.7$ mag.

2.3 The re-ignition of the compact jets

Figure 2 shows the multi-wavelength lightcurves of GX 339−4 during the decay of its 2010-11 outburst. The dashed line indicates the increase of the hard X-ray emission on MJD 55594 associated with the transition of GX 339−4 back to the hard state (see Dinçer et al. 2012). Radio emission from the compact jets is quenched in the soft state (Fender et al. 1999). Due to the increased sensitivity of the ATCA array and denser coverage, we fully observe, for the first time, the recovery of the radio emission during the soft to hard state transition when the compact jets are building up. Despite sparse initial coverage, the onset of radio emission from GX 339−4 is clearly observed. It occurs in conjunction with the increase of hard X-ray emission (Fig. 2). The peak of radio emission is concomitant with the peak in hard X-rays, as well as with the rise of the OIR emission. However, the overall shape of the reflares are different with,

e.g., the hard X-rays appearing to be more symmetric than the radio peak. The peak flux in OIR is reached ~ 2 weeks after the maximum of radio emission. The timescale to reach the peak emission (assuming a transition on MJD 55594) is much longer (~ 17 days) in OIR compared to hard X-rays (~ 10 days), and maybe also compared to radio. We note that the transition may have even started in radio and X-ray as early as MJD 55578, if we consider the weak radio detection (see Table 2 online) that is consistent with the leveling off of the X-ray timing properties (Dinçer et al. 2012).

If we define the radio flux density, F_ν, as $F_\nu \propto \nu^\alpha$ (with α the spectral index), we note a clear change, after the transition to the hard state (Fig. 2), from a negative spectral index to a saturation around $\sim +0.4$. This trend corresponds to an evolution from optically thin to optically thick synchrotron emission, associated with the building up of the compact jets during the state transition. Connecting the radio measurements to the two *Herschel* observations at 70 μm allows us to precisely characterise the radio to far-IR spectral indices to 0.32 ± 0.01 on Feb. 25th and 0.38 ± 0.01 on Mar 6th, which is fully consistent with the radio estimates (Fig. 2). The detections by *Herschel* of a variable source at the location of GX 339−4 during a hard state further indicate that this far-IR emission is likely related to the self-absorbed compact jets of GX 339−4.

3 DISCUSSION

Our campaign during the decay of the 2010-11 outburst of GX 339−4 allowed us to obtain for the first time a significant detection of the compact jets in the far-IR with *Herschel*, as well as to observe the full recovery of the compact jets in radio and OIR. This enables us to bridge the 4-decade frequency gap between the radio and OIR domains.

3.1 Formation of the compact jets

Inspection of the evolution of the broadband spectra (Fig. 3) demonstrates that the compact jets are first detected at radio frequencies as optically thin synchrotron emission (# 1 and 2). The radio spectrum becomes flat (Fig. 2 (bottom)) after the onset of the OIR reflare and its spectral index then increases up to a value of the order of +0.40, at a time when the OIR peaks and starts to decay. Such sequence has not been documented before in as much details (e.g. the 1999 decay of GX 339−4, Corbel et al. 2000), especially in light of the evolution of the radio emission during the soft to hard state transition. However, the previous studies that discuss some radio and/or OIR observations (Kalemci et al. 2005, 2006; Brocksopp et al. 2005; Fender, Homan & Belloni 2009; Miller-Jones et al. 2011; Dinçer et al. 2012; Miller-Jones et al. 2012) are consistent with our new findings. The comparative evolution of the radio and OIR lightcurves clearly points to a delay (~ 2 weeks) between these two domains (see also Coriat et al. 2009). In fact, this is consistent with the reverse trend that is observed during the hard to soft state transition, with an initial quenching (by one to two weeks) of the NIR emission (Homan et al. 2005; Russell et al. 2008; Coriat et al. 2009; Buxton et al. 2012; Yan & Yu 2012).

In the model of self-absorbed compact jets

(Blandford & König 1979; Falcke & Biermann 1995) adapted for stellar mass BHs (e.g. Markoff, Nowak & Wilms 2005), the OIR emission arises from closer to the base of the jets, whereas the radio emission comes further down the jets. The observed delay between OIR and radio emission during the formation is not consistent with any travel time within the jets. We still do not fully understand the internal processes in jets leading to particle acceleration and ultimately radiation. However, this delay is likely associated with the timescale for building up turbulences and strong shocks along an extended zone in the magnetized jet plasma, as well as for reaching high enough densities for the flow to become optically thick at OIR frequencies. One can imagine the following scenario to explain the evolution of the broadband spectra. Once the jets are launched, an initial zone of particle acceleration, associated with the first shocks, forms. While the density of the jet plasma is still low, this results in an optically thin synchrotron power-law spectrum peaking in the radio band. As the density in the jets increases, this leads to a transition to higher optical depth. At the same time, pile-up of the flow or internal shocks (Malzac 2012) build up and cause particle acceleration to occur closer to the base of the jets. Alternatively, an increase in particle acceleration efficiency at the jet base could also boost the energy of the particles, giving rise gradually to enhanced synchrotron emission up to OIR.

One would therefore expect the observed behaviour: a transition from a steep to a flat spectrum with an evolution of the peak power from radio to NIR. A reverse scenario (decrease in the particle densities and/or the efficiency of particle acceleration) would also be consistent with the trend (initial OIR quenching) observed during the hard to soft state transition. The onset of radio emission can thus be seen as a tracer (better than OIR) of the jets re-ignition, while the broadband evolution leading to inverted synchrotron spectrum peaking in the OIR traces the development of the jets power and their internal structure during outbursts.

3.2 On the far- to near-infrared emission

The very good sensitivity of the *Herschel*/PACS instrument and of the upgraded ATCA demonstrates that the far-IR emission of GX 339−4 is clearly and significantly above a simple extrapolation of the radio to NIR spectrum (see broadband spectral evolution in Fig. 3 during the phase of compact jets formation). This is in contradiction with the usual assumption of a simple powerlaw (e.g. Markoff, Nowak & Wilms 2005) with a turnover frequency in the mid to near-IR range. Subtracting the thermal component in the OIR would further increase the far-IR emission relative to the OIR. This is in fact reminiscent of the 850 μm (350 GHz) JCMT detection of XTE J1118+480 in 2000 (Fender et al. 2001), which was also clearly above the radio to OIR inverted spectrum (see their Fig. 2). The radio to sub-millimeter spectral index of +0.5 for XTE J1118+480 is furthermore quite comparable with the value measured during our *Herschel* observations of GX 339−4 (Fig. 2). V404 Cyg may display occasionally a similar broadband spectra (Russell et al. 2012b).

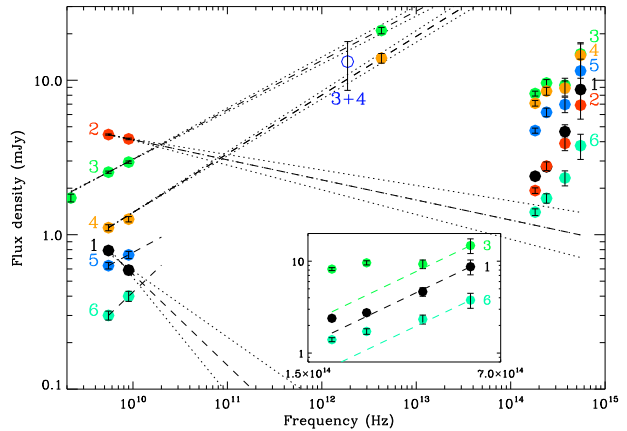These three sources seem to point out a more complex broadband spectra for the compact jets during some

Figure 3. Evolution of the radio to OIR broadband spectra during the soft to hard state transition. The numbers (and associated colors) refer to the epochs highlighted in Fig. 2. The dashed lines corresponds to the extrapolation of the radio spectra (with dotted lines to indicate the 1-σ error when it is not too large). For the spectra # 3 and 4 (which includes the *Herschel* observations), we use the measured radio to far-IR spectral index. The open blue circle is the 160 μm detection combining the two *Herschel* observations. Inset: Zoom of the OIR spectra # 1, 3 and 6. The dashed lines correspond to an extrapolation of the V-band with an index of +1.5 (possible for an irradiated disk, Hynes 2005) for a selection of the spectra.

epochs. The optically thick synchrotron emission from the jets manifests itself by an inverted power-law from the radio up to at least the far-IR (same spectral index, Fig. 2). The turnover frequency during our two *Herschel* observations is likely above 5×10^{12} Hz, which is consistent with previous estimates. It is clear from the evolution of the OIR lightcurves (Fig. 2 and also Dinçer et al. 2012) that most of the NIR emission during the reflare is not from the intrinsic decaying thermal emission from the accretion disk. Furthermore, this OIR reflare can not be completely due to the optically thin synchrotron emission from the compact jets, because it displays a rather flat spectra (after subtraction of the thermal emission) according to Dinçer et al. (2012). This means that another emission process may dominate the OIR range (see also Rahoui et al. 2012; Dinçer et al. 2012). Even if the OIR reflare is delayed compared to the radio synchrotron emission, this OIR emission could still be related to the jets via, e.g., pre-shock synchrotron from the thermal particles at the base of the jets (Markoff, Nowak & Wilms 2005). The OIR could also be affected by an episode of particle acceleration in the jets in a particularly strong magnetic field (Pe'er & Casella 2009). Alternatively, the OIR excess may be related to synchrotron emission from the hot accretion flow (Veledina, Poutanen & Vurm 2011). At first sight, the shape of the OIR spectra (see inset in Fig. 3) could also possibly highlight, as a viable alternative mechanism, the role of irradiation of the disk (Hynes 2005) by the jets, which form during this period.

With optically thick synchrotron emission in the 10^9 - 5×10^{12} Hz (~ 70 μm) range and assuming a radiative efficiency of ϵ=0.05 [see discussion in Corbel & Fender (2002), or recently in Nemmen et al. (2012) who suggest that ϵ could be as high as 0.15], we obtain a likely lower limit on the

power of compact jets during *Herschel* observations #1 of $\sim 10^{35}$ erg s^{-1}. Adding an optically thin jet component (of spectral index –0.6) in the 5×10^{12} to 10^{14} Hz increases the jet power to $\sim 10^{36}$ erg s^{-1}. This corresponds to at least 17 % of the 0.1-200 keV luminosity (6×10^{36} erg s^{-1} for a distance of 8 kpc), a significant fraction of the accretion power (assuming no correction for bulk relativistic motion). This probably implies that the jet spectral break can not be much higher than the frequency of the *Herschel* observations. For a comparison, in the brighter hard state during the rise (with an X-ray luminosity of 1.5×10^{38} erg s^{-1}), Gandhi et al. (2011) measured this break at $\sim 5 \times 10^{13}$ Hz. A jet frequency break moving to lower frequency is expected as the mass accretion is reduced during the outburst decay (Heinz & Sunyaev 2003; Falcke, Körding & Markoff 2004; Russell et al. 2012b). Furthermore, the *Herschel* measurements would translate into a magnetic field strength of $\sim 2 \times 10^3$ G in the acceleration zone and a jet cross section radius of $\sim 10^{10}$ cm (Chaty, Dubus & Raichoor 2011). These numbers would eventually imply compact jets with weaker magnetic field and a larger base during the decaying hard state compared to the rising hard state observed by Gandhi et al. (2011) (if we take the same assumptions).

To summarize, our new campaign highlights a much more complicated radio to OIR spectral shape than usually assumed, especially around the time of the transition. However, on many occasions, the OIR measurements may still lie on the extrapolation of the radio spectrum (e.g. Coriat et al. 2009; Buxton et al. 2012). This reinforces the need for new observations, e.g. with the ALMA array or with sensitive mid to far IR observations, to bridge the gap between the radio and the OIR domains and constrain the evolution of the jets SED and power during BH outbursts.

REFERENCES

Blandford R. D., Königl A., 1979, ApJ, 232, 34
Brocksopp C., Corbel S., Fender R. P., Rupen M., Sault R., Tingay S. J., Hannikainen D., O'Brien K., 2005, MNRAS, 356, 125
Buxton M. M., Bailyn C. D., 2004, ApJ, 615, 880
Buxton M. M., Bailyn C. D., Capelo H. L., Chatterjee R., Dinçer T., Kalemci E., Tomsick J. A., 2012, AJ, 143, 130
Casella P. et al., 2010, MNRAS, 404, L21
Chaty S., Dubus G., Raichoor A., 2011, A&A, 529, A3
Corbel S., Coriat M., Brocksopp C., Tzioumis A. K., Fender R. P., Tomsick J. A., Buxton M. M., Bailyn C. D., 2012a, ArXiv e-prints
Corbel S. et al., 2012b, MNRAS, 421, 2947
Corbel S., Fender R. P., 2002, ApJ, 573, L35
Corbel S., Fender R. P., Tzioumis A. K., Nowak M., McIntyre V., Durouchoux P., Sood R., 2000, A&A, 359, 251
Coriat M., Corbel S., Buxton M. M., Bailyn C. D., Tomsick J. A., Körding E., Kalemci E., 2009, MNRAS, 400, 123
Dinçer T., Kalemci E., Buxton M. M., Bailyn C. D., Tomsick J. A., Corbel S., 2012, ApJ, 753, 55
Falcke H., Biermann P. L., 1995, A&A, 293, 665
Falcke H., Körding E., Markoff S., 2004, A&A, 414, 895
Fender R., 2006, Jets from X-ray binaries, Compact stellar X-ray sources, pp. 381–419
Fender R. P., 2001, MNRAS, 322, 31
Fender R. P. et al., 1999, ApJ, 519, L165
Fender R. P., Hjellming R. M., Tilanus R. P. J., Pooley G. G., Deane J. R., Ogley R. N., Spencer R. E., 2001, MNRAS, 322, L23
Fender R. P., Homan J., Belloni T. M., 2009, MNRAS, 396, 1370
Gallo E., Migliari S., Markoff S., Tomsick J. A., Bailyn C. D., Berta S., Fender R., Miller-Jones J. C. A., 2007, ApJ, 670, 600
Gandhi P. et al., 2011, ApJ, 740, L13
Heinz S., Sunyaev R. A., 2003, MNRAS, 343, L59
Hjellming R. M., Gibson D. M., Owen F. N., 1975, Nature, 256, 111
Homan J., Buxton M. M., Markoff S., Bailyn C. D., Nespoli E., Belloni T., 2005, ApJ, 624, 295
Hynes R. I., 2005, ApJ, 623, 1026
Hynes R. I., Steeghs D., Casares J., Charles P. A., O'Brien K., 2003, ApJ, 583, L95
Jain R. K., Bailyn C. D., Orosz J. A., McClintock J. E., Remillard R. A., 2001, ApJ, 554, L181
Kalemci E., Tomsick J. A., Buxton M. M., Rothschild R. E., Pottschmidt K., Corbel S., Brocksopp C., Kaaret P., 2005, ApJ, 622, 508
Kalemci E., Tomsick J. A., Rothschild R. E., Pottschmidt K., Corbel S., Kaaret P., 2006, ApJ, 639, 340
Laurent P., Rodriguez J., Wilms J., Cadolle Bel M., Pottschmidt K., Grinberg V., 2011, Science, 332, 438
Lutz D., 2012, PACS photometer point spread function. Tech. Rep. PICC-MR-TN-033, MPE
Malzac J., 2012, MNRAS, L13
Markoff S., Nowak M. A., Wilms J., 2005, ApJ, 635, 1203

Migliari S. et al., 2007, ApJ, 670, 610

Miller-Jones J. C. A., Jonker P. G., Maccarone T. J., Nele-
mans G., Calvelo D. E., 2011, ApJ, 739, L18

Miller-Jones J. C. A. et al., 2012, MNRAS, 421, 468

Mirabel I. F., Rodriguez L. F., Cordier B., Paul J., Lebrun
F., 1992, Nature, 358, 215

Muñoz-Darias T., Casares J., Martínez-Pais I. G., 2008,
MNRAS, 385, 2205

Nemmen R. S., Georganopoulos M., Guiriec S., Meyer
E. T., Gehrels N., Sambruna R. M., 2012, ArXiv e-prints

Pe'er A., Casella P., 2009, ApJ, 699, 1919

Pilbratt G. L. et al., 2010, A&A, 518, L1

Poglitsch A. et al., 2010, A&A, 518, L2

Rahoui F. et al., 2012, MNRAS, 422, 2202

Rahoui F., Lee J. C., Heinz S., Hines D. C., Pottschmidt
K., Wilms J., Grinberg V., 2011, ApJ, 736, 63

Russell D. M. et al., 2012a, MNRAS, 419, 1740

Russell D. M., Maitra D., Fender R. P., Lewis F., 2008, in
Microquasars and Beyond

Russell D. M. et al., 2012b, ArXiv e-prints

Veledina A., Poutanen J., Vurm I., 2011, ApJ, 737, L17

Yan Z., Yu W., 2012, MNRAS, L523

Zdziarski A. A., Gierliński M., Mikołajewska J., Wardziński
G., Smith D. M., Harmon A. B., Kitamoto S., 2004, MN-
RAS, 351, 791